

Article

Rich CuO Nanowires Fabrication via Laser Post-Treatment of Laser-Textured Copper Substrate

Zhekun Chen ^{1,†} , Gongfa Yuan ^{1,†}, Rui Zhou ^{1,2,*} , Weipeng Huang ¹ and Minghui Hong ^{1,2,*}¹ School of Aerospace Engineering, Xiamen University, Xiamen 361005, China² Innovation Laboratory for Sciences and Technologies of Energy Materials of Fujian Province (IKKEM), Xiamen 361005, China

* Correspondence: rzhou2@xmu.edu.cn (R.Z.); elehmh@xmu.edu.cn (M.H.)

† These authors contributed equally to this work.

Abstract: The superhydrophobic and anti-icing properties of copper-based materials have been widely concerned. Laser texturing followed by thermal oxidation is a method to prepare durable CuO nanowires on Cu substrate. Rich CuO nanowires on micro-structures are required to meet its applications for anti-icing based on sustaining better Cassie–Baxter state stability. In this paper, dense CuO nanowires are obtained by additional laser post-treatment between the laser texturing and thermal oxidation. Uniform Cu₂O and CuO layers form on the micro-structures by the laser post-treatment, which serves as the precursors for the growth of nanowires. The density of CuO nanowire increases from 44.3% to 61.4%, resulting in excellent superhydrophobicity and anti-icing performance. The delayed freezing time increases from 17 s to 1519 s at the temperature of -10 °C, which is more than 80 times longer compared to pure Cu substrate. The resulting anti-icing property shows durability through icing–melting cycles and taping tests. This feasible method opens new possibilities for enhanced anti-icing property on copper-based equipment used in low-temperature environments.

Keywords: CuO nanowires; laser treatment; thermal oxidation; anti-icing; superhydrophobicity



Citation: Chen, Z.; Yuan, G.; Zhou, R.; Huang, W.; Hong, M. Rich CuO Nanowires Fabrication via Laser Post-Treatment of Laser-Textured Copper Substrate. *Inorganics* **2022**, *10*, 236. <https://doi.org/10.3390/inorganics10120236>

Received: 12 October 2022

Accepted: 30 November 2022

Published: 2 December 2022

Publisher's Note: MDPI stays neutral with regard to jurisdictional claims in published maps and institutional affiliations.



Copyright: © 2022 by the authors. Licensee MDPI, Basel, Switzerland. This article is an open access article distributed under the terms and conditions of the Creative Commons Attribution (CC BY) license (<https://creativecommons.org/licenses/by/4.0/>).

1. Introduction

Copper and its alloys are widely used in daily life, such as in buildings [1], ocean engineering [2], and aircraft [3], owing to their high electrical conductivity, thermal conductivity, corrosion resistance, and some unique other physical and chemical properties. In low-temperature conditions, water molecules are easy to aggregate and freeze on the copper-made components due to their high surface energy [4,5], which brings serious side effects on the stability and property of equipment [6–12]. Traditional anti-icing/deicing methods are developed based on active strategies, such as using thermal [13,14], over-current [15], short circuit [16], loading [17], high-frequency pulse current heating oscillation, and laying heating conductors [18], which lead to excessive energy consumption. Hence, many researchers [19–22] focus on superhydrophobic surfaces for enhancing anti-icing as a passive strategy by decreasing heat transfer efficiency to delay the nucleation of water and reduce the icing adhesion. Superhydrophobic materials can remain entirely ice-free down to -25 to -30 °C, due to their ability to repel impacting water before ice nucleation occurs [19]. Jiang et al. [4] fabricated the different microstructures on copper substrate via a femtosecond laser, which delayed the ice formation at temperatures of -5 °C and -10 °C.

Recently, many methods have been developed to obtain superhydrophobicity on copper-based surfaces mainly including wet chemical etching, oxidation, electrodeposition, and immersion [23–26]. Limited by durability and other shortcomings, it has not been promoted and widely used. Laser texturing is a promising approach to structure metal surfaces precisely to enhance their functional performances [27–29]. Combined with thermal oxidation, it is considered to be an effective method for constructing durable micro/nano-structures on the copper surfaces. Xu et al. [30] employed nanosecond laser ablation on

Cu sheet coupled with subsequent thermal oxidation to form hedgehog-like, high-density, and dual-scale micro/nano-structures, which exhibit boosted interfacial adhesion with favorable stability. Khew et al. [31] presented the use of a pulsed 1064 nm laser texturing to significantly improve the adhesion and sturdiness of CuO nanowires array on Cu foil with laser fabricated micro-holes. Yan et al. [32] achieved stable superhydrophobicity on Cu with apparent advancing contact angles of 160° and contact angle hysteresis as low as 20° by utilizing the laser processing and thermal oxidation of copper, followed by repeatable and passive atmospheric adsorption of hydrophobic volatile organic compounds. Such works demonstrate the feasibility of the method of laser texturing combined with thermal oxidation to fabricate durable micro/nano-structures on Cu substrate to meet specific application requirements.

Rich CuO nanowires are required on the surfaces of micro-structures to sustain hydrophobicity at sub-zero temperatures for enhancing the anti-icing property. In this paper, laser post-treatment is coupled between the laser texturing and thermal oxidation to fabricate dense nanowires. The additional processing improves the density of nanowires. The enhanced anti-icing performance of as-prepared samples is revealed by delaying the freezing time of droplets effectively at a low temperature. The function and morphology of the surface are proved to be durable and robust via icing–melting cycles and tape tests. The rich CuO nanowires endowed with the facile fabrication strategy, enhanced anti-icing performance, as well as boosted durability, initiate the path toward new applications at a low temperature.

2. Results

2.1. Surface Morphology and Wettability

As shown in Figure 1, a micro-column array is fabricated by laser texturing on Cu substrate. Then, one group of samples is directly treated by thermal oxidation as a control group. The other group is processed by an additional laser post-treatment. Two representative samples are compared with same processing parameters in laser texturing and thermal oxidation.

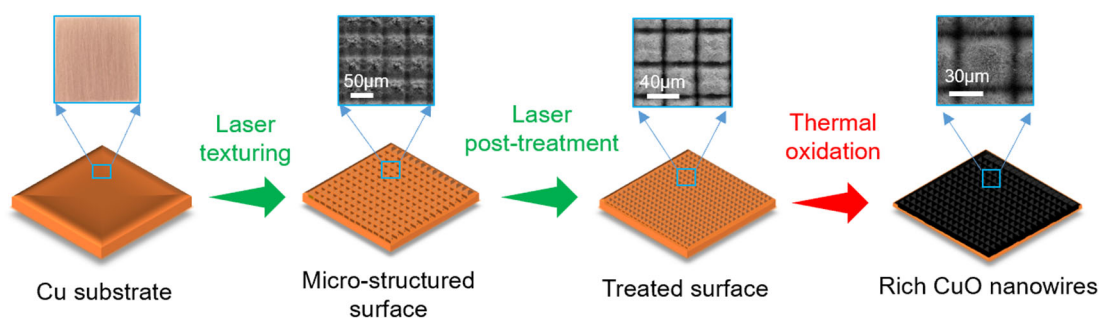


Figure 1. Schematic of rich CuO nanowire fabrication via laser texturing, laser post-treatment, and thermal oxidation (LT-LPT-TO).

The SEM images of the 50LT-4TO and 50LT-LPT-4TO samples are shown in Figure 2a, which shows the difference in surface topography with or without the laser post-treatment. It can be seen from Figure 2(ai) that the CuO nanowires grow well in the laser texturing region. However, on the upper surface of the micro-column, the CuO nanowires do not grow all over the surface. In the laser texturing process, compressive forces can be created by the vapor and plasma plume, leading to the expulsion of a molten pool of materials. A portion of the liquefied material is resolidified and accumulates to cover the surrounding non-processed areas. However, this process cannot form uniform CuO and Cu₂O layers on the upper surface of the micro-column, which is key to promote the growth of CuO nanowires, for example, in the defective areas marked on the SEM image, the CuO nanowires barely grow. In Figure 2(aii), the laser post-treatment is coupled to modify the textured surface. The defective areas are significantly reduced or even disappear on the

upper of the micro-column and are covered by CuO nanowires. In the insets, the statistical images demonstrate the density of nanowires, which increases from 44.3% to 61.4%. In addition, processing parameters in laser texturing and thermal oxidation are optimized to obtain better superhydrophobicity and anti-icing performance. The SEM images of all samples with different surface morphologies are shown in Figure S1, with the influence of different scanning intervals on surface morphology at the same heating time (4 h). Three parameters of scanning intervals are selected as 30 μm (30LT), 50 μm (50LT), and 60 μm (60LT). Different scanning intervals lead to micro-columns with different sizes, which are the base for the growth of CuO nanowires. Figure S1a shows that the upper surface of the micro-column cannot be modified by laser texturing and the CuO nanowires grow sparse with the increase in scanning interval. It can be observed in Figure S1b that the nanowires on the top of the micro-column are denser after the laser post-treatment in different processing parameters. Figure S2 shows the influence of different thermal oxidation time at the same scanning interval (50 μm). With the increase in heating time, the CuO nanowires grow longer on the surface of the micro-column. As shown in Figure 2b, the diameter and length of CuO nanowires of the 50LT-LPT-4TO sample are about 50 nm and 7 μm , respectively. The CuO nanowires cannot cover all upper surface of the micro-column. It is concluded that the laser texturing samples cannot grow rich CuO nanowires on the upper surface of the micro-columns by regulating the laser scanning interval and heating time. It is attributed to little modifications of the micro-column surface by laser texturing. The Cu_2O and CuO layers cannot fully form, whose presences are the key to promote the growth of nanowires. From the oblique view in Figure S3, the length and density of the nanowires can be estimated at a tilting angle of 40° . A comparison with the surface topography without the laser post-treatment is presented in Figure S4. The laser post-treatment makes the roughness of the micro-column upper surfaces decrease significantly as shown in Figure S5. The structures are changed by the laser post-treatment, which is beneficial to the growth of CuO nanowires. Especially on the upper surface of the laser textured micro-column, the laser post-treatment makes the CuO and Cu_2O layers fully grow over the surface, which serves as the precursors for the growth of nanowires [31]. In Figure S6, the depths of the 50LT and 50LT-LPT samples are measured as about 56.9 μm and 42.5 μm , respectively. It indicates that laser post-treatment ablates the rough structures on the upper surface of the micro-column. Meanwhile, the increase in nanowires on different samples is demonstrated by statistical images in Figure S7. It is concluded that the additional laser post-treatment increases the density of the CuO nanowires.

The wettability changes with or without the laser post-treatment are shown in Figure 2c. The CA and SA are measured after the IPA treatment, which obtains the low surface-energy in a short time. The wettability without the laser post-treatment is greater, in which the water droplet sticks on the surface. The possible reason is that some areas on the upper surface of the micro-column cannot be modified by the laser texturing, causing a lower density of CuO nanowires. The defective area without the nanowires has high adhesion to droplets, which shows the Wenzel state [33], causing great wettability. The shaded portion of the bars shows the change in wettability after the laser post-treatment. In general, the wettability of all samples is obviously decreased. The superhydrophobicity can be achieved at every laser scanning interval and heating time after the laser post-treatment. The SA becomes significantly lower due to rich CuO nanowires on the micro-column surface, which indicates that the water droplet appears as the Cassie–Baxter state [34,35] with air in micro-structures. The CA increases and then decreases with the change of thermal oxidation, reaching the peak value at the heating time of 4 h. Combined with SEM images in Figure S2, the length of many CuO nanowires on the micro-column surface can be estimated as 5 μm when the heating time is 6 h. The wettability is decreased slightly. Similarly, the SA gradually decreases at first, reaches the peak value, and then increases with thermal oxidation time. The CuO nanowires grow longer as the thermal oxidation time increases, causing the SA to increase. It may be because too long nanowires limit the water droplet to roll off. When the scanning interval is 50 μm and the heating time

is 4 h, the wettability can be optimized with a CA of 164° and a SA of 2° . Regulating the laser scanning interval and heating time cannot achieve superhydrophobicity on the surface without the laser post-treatment. Coupling the laser post-treatment between the laser texturing and thermal oxidation could significantly decrease the wettability.

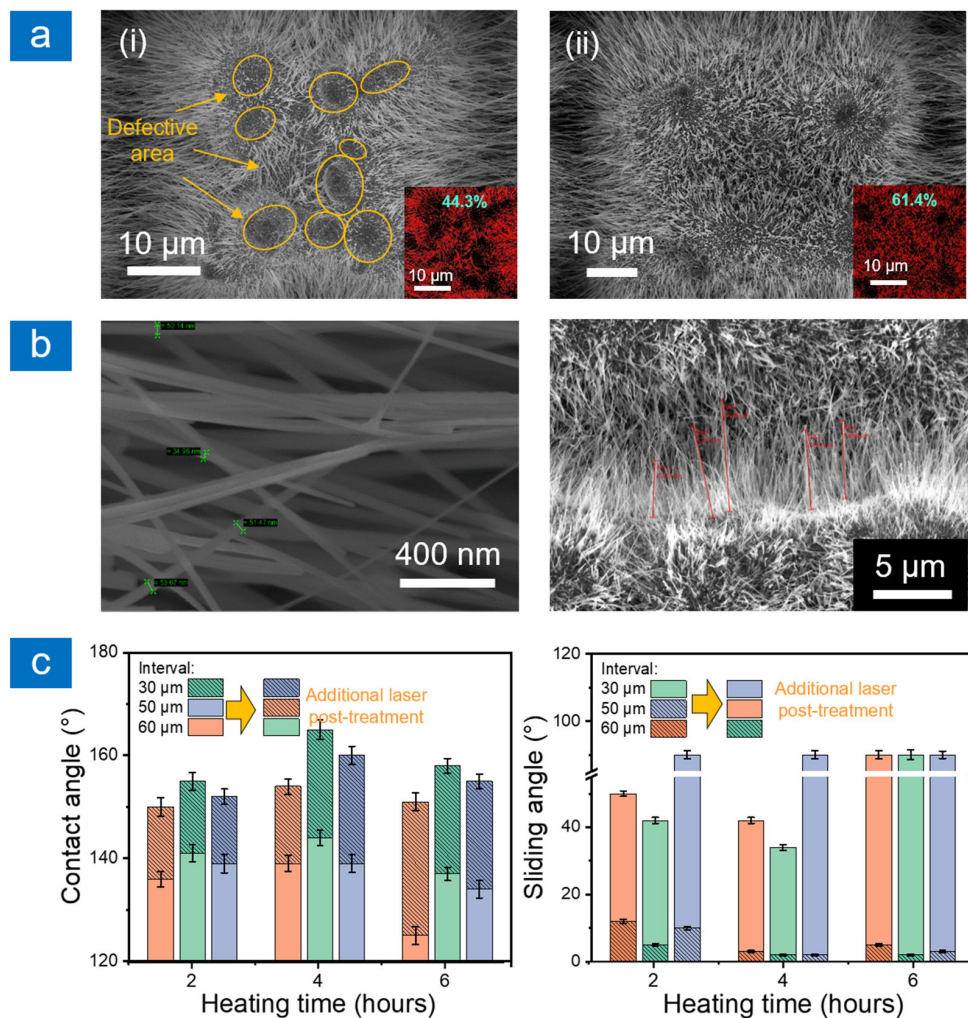


Figure 2. (a) SEM images of surface morphology by laser texturing and thermal oxidation (i) without and (ii) with laser post-treatment. (b) Diameter and length of CuO nanowires of 50LT-LPT-4TO sample. (c) Comparison of surface wettability: contact angles on the left chart and sliding angles on the right chart.

Thermal oxidation is used to grow CuO nanowires. As shown in Figure 3a, after the laser processing of Cu substrates, a layered structure is formed, including CuO in the top layer, Cu₂O in the middle layer, and Cu sheet at the bottom [36]. Compressive stress is generated in the lower surfaces of the Cu₂O/CuO layer resulting in a stress gradient from the Cu-Cu₂O interface. Cu atoms migrate from the Cu-Cu₂O interface to the CuO-air interface as the oxidation continues. Stress-driven grain boundary diffusion induces the growth of nanowires on the Cu surface. Cu atoms diffuse subsequently along nanowires, simultaneously react with the oxygen, and form new CuO at the tips of CuO nanowires [37–39]. Therefore, the formation of CuO and Cu₂O layers is important for the growth of nanowires. Without laser post-treatment, Cu atoms will diffuse toward the laser-textured area rather than the upper surface of the micro-structure. In Figure 3b, the surfaces are characterized via EDS. The content of oxygen is increased after laser post-treatment, which supports the formation of the Cu₂O/CuO layer. Laser post-treatment forms homogenized layers resulting in denser growth of nanowires. The heating temperature and time are impor-

tant parameters to control the growth process, which affects the morphology of CuO nanowires [39–42]. The heating temperature of CuO NWs is set as 550 °C and the heating time varies from 2 to 6 h to form different lengths. Traditional thermal oxidation technology has a serious problem in that the thermal stress [43] caused by high-temperature heating may lead to the cracking of CuO nanowires films. In the process of thermal oxidation of the pure copper surface, the newly generated CuO nanowires/layer will likely fall off directly in the cooling process due to the relatively fast cooling rate. The micro/nano-structure is constructed firstly via laser texturing, which releases the thermal stress into the free space, reduces the generation of thermal stress, and prevents cracking and stripping, which obviously reduces the risk of shedding the oxide layers [31]. Uniform Cu₂O and CuO layers are fully formed by the laser post-treatment [43], which exist in the form of precursors in the growth process of CuO nanowires. The micro/nano-structure morphology of the substrate affects the initial position and growth direction of nanowires. Therefore, even if the thermal oxidation parameters are the same, different micro-structures can form nanowires with different densities. Due to the change in the growth of nanowires, the diffusion of Cu atoms in the oxidation is also affected. Therefore, the laser post-treatment is coupled to make CuO and Cu₂O layers more uniform on the micro-structures, leading to rich and dense nanowires growth.

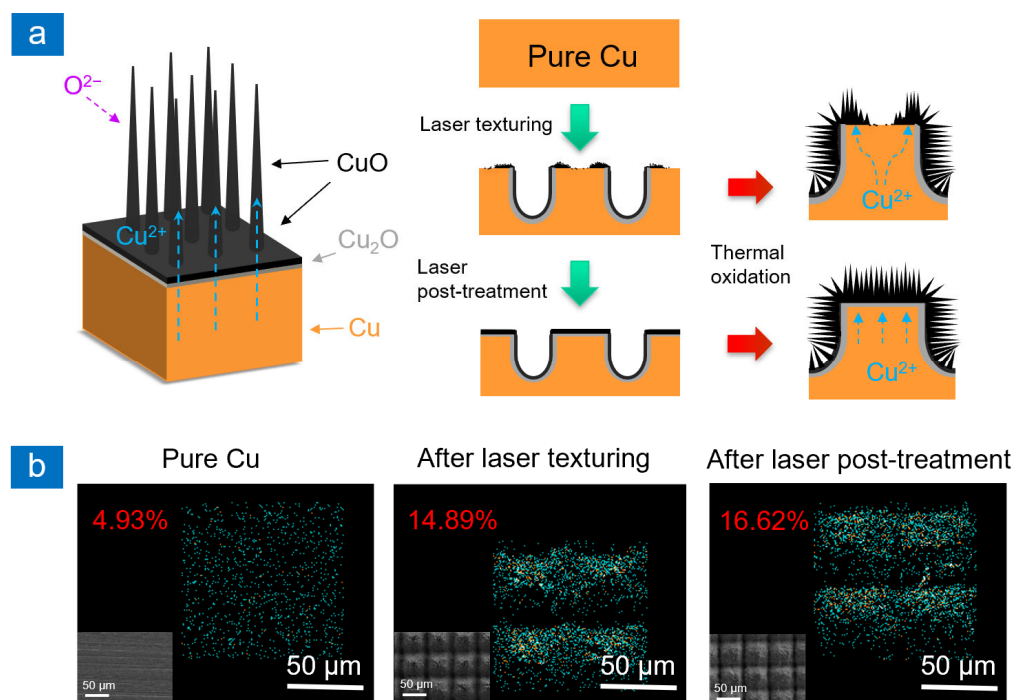


Figure 3. (a) Growth mechanism of CuO nanowires on surface without or with the laser post-treatment. (b) EDS images of oxygen atomic percent and corresponding morphologies.

2.2. Anti-Icing Performance

The delayed freezing time is recorded to assess the anti-icing abilities of different samples on a self-made cryogenic test platform. Figure 4a shows the freezing process of water droplets on the surface of pure Cu, 50LT-4TO, and 50LT-LPT-4TO samples. On the pure Cu surface, the droplet rapidly begins to freeze at 14 s and complete freezing at 17 s as the temperature of the cooling platform is −10 °C. The CA of the pure Cu surface is 61° which means a large contact area between substrate and water. It increases heat loss from water droplet to the cold substrate. The 50LT-4TO sample has a better hydrophobic performance. The delayed freezing time is extended to 44 s, which is nearly three times longer compared to the pure Cu. After the laser texturing and thermal oxidation, plenty of micro-column arrays and CuO nanowires form on the surface. However, CuO nanowires

grow incompletely on the upper surface of the micro-column. The morphology feature of the upper surface has more influence on the solid–liquid contact area. Combining with the wettability, the value of SA indicates the droplet is in the transitional state between the Wenzel model and the Cassie–Baxter model. When the temperature decreases, the wettability deteriorates and the state changes to the Wenzel model, shortening the freezing time of the droplet. The 50LT–LPT–4TO sample increases the start freezing time to 1470 s, which is 105 times longer than pure Cu and 43 times longer than the 50LT–4TG sample. The laser post-treatment is a key process to perfect the morphology of nanowires on the upper surface of the micro-column for enhancing the anti-icing property. As can be seen in Figure 4a, the water droplet always closes to a circular shape during the whole freezing process and only changes slightly after completely freezing. The delayed freezing times for different laser processing parameters are shown in Figure 4b. The laser post-treatment visibly extends the freezing time of water droplets on the sample surface. Dense CuO nanowires on the upper surface of the micro-column support water droplets to retain the Cassie–Baxter state. In the Cassie–Baxter state, trapped air in micro/nano-structures plays a role as thermal resistance, reducing the heat loss from the droplet to the sample surface and significantly prolonging the freezing time of the droplet [22]. When the laser scanning interval and thermal oxidation are optimized, the density and length of CuO nanowires are optimal, and the support for water droplets achieves the best effect.

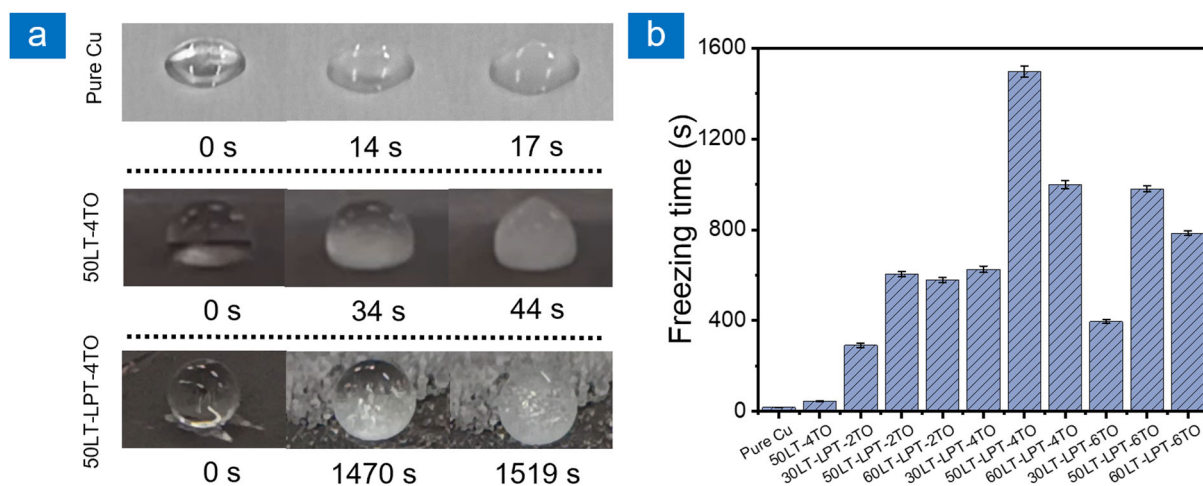


Figure 4. Anti-icing performances of different samples at a surface temperature of $-10\text{ }^{\circ}\text{C}$. (a) Freezing process of a single droplet on different samples. (b) Delayed freezing time of different samples.

2.3. Durability

In practical applications, icing and melting processes occur many times in long service life. Long-term effective anti-icing property should be considered as a challenge to superhydrophobic surfaces. In this work, the icing–melting cycle is tested to verify the durability of CuO nanowires. The water droplet is frozen, melted, and removed by a compressed air spray gun on the 50LT–LPT–4TO sample as one cycle of test. A total of 10 cycles are repeated to observe the change in wettability and delayed freezing time in Figure 5a. After icing and melting cycles, the CA of the sample surface and the freezing time of a single droplet do not change significantly. It indicates that the CuO nanowires prepared by coupling the laser post-treatment can withstand the change in temperature and ensure stability.

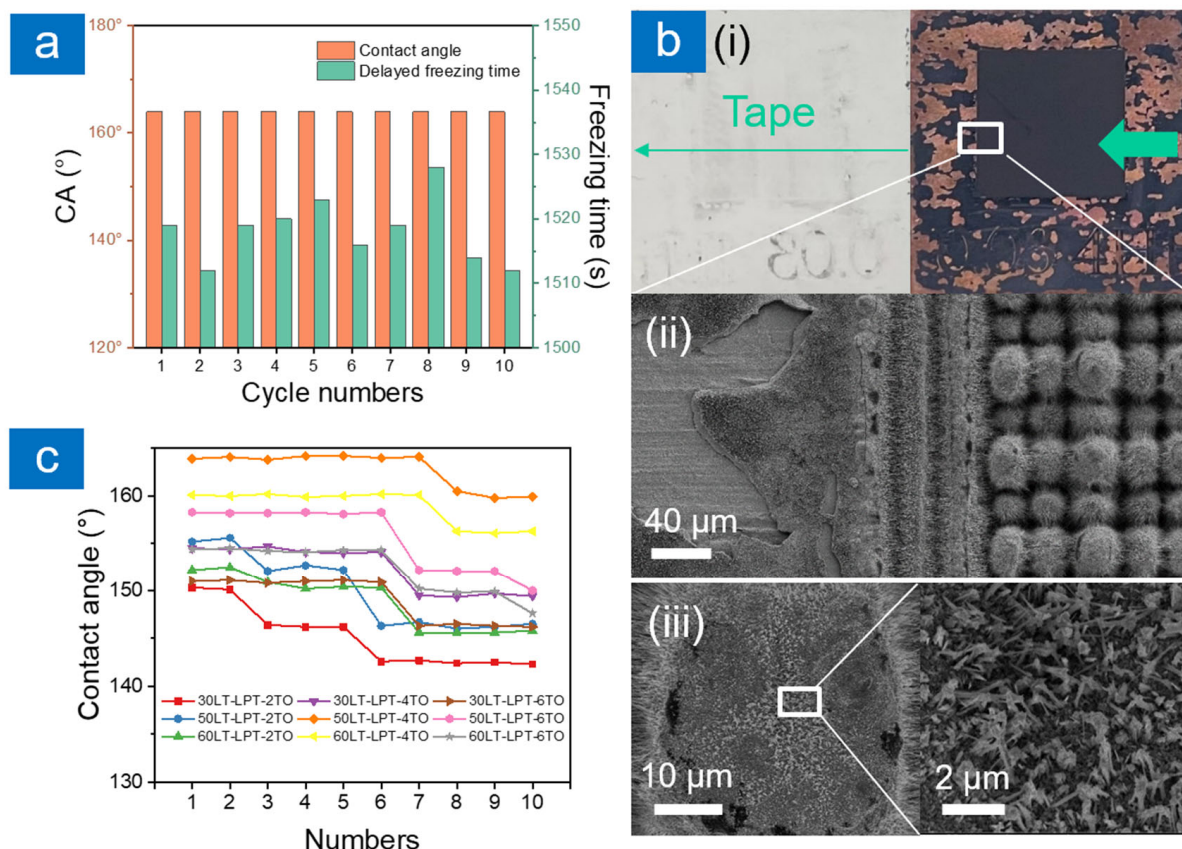


Figure 5. Durability tests. (a) Variations of wettability and anti-icing performance in icing–melting cycles for the 50LT-LPT-4TO sample. (b) Tape test: (i) optical microscopic image; (ii,iii) SEM images of the 50LT-LPT-4TO sample after 10 cycles. (c) Variation of contact angle with number of tape test cycles.

Industrial applications often require surfaces to be durable in harsh operating environments. To further prove the durability of the CuO nanowires, the tape test is carried out on different samples, as shown in Figure 5b. In Figure 5(bi), some black parts are found on the tape as the CuO nanowires fall off from the sample. Most of the CuO nanowires on the original copper surface fall off and the textured region is relatively intact, as shown in Figure 5(bii). As can be seen from Figure 5(biii), some root parts of the CuO nanowires remain on the upper surface of the micro-column after breaking. After the tape tearing, one part of the nanowires still bond to the substrate, which makes the surface remain superhydrophobic. The tape is attached to the sample surfaces, then removed at a slow speed to complete one cycle of test. The CAs of different samples are then measured after each cycle. It can be seen from Figure 5c that the CA of each sample does not decrease sharply with the test cycles. Only the CAs of the samples fabricated by 2-h thermal oxidation decrease slightly in six cycles. The CAs of all samples decrease after seven cycles. The adhesion of CuO nanowires grown on the copper surface is significantly improved after the laser post-treatment. For the conventional thermal oxidation growth, the generated CuO nanowires film falls off easily due to the low adhesion caused by thermal stress. In our method, the micro/nano-structure is constructed firstly via laser ablation, which releases the thermal stress, reduces the generation of thermal stress, and prevents cracking and stripping. It significantly reduces the risk of shedding the oxide layers and makes the surface robust and durable. The improvement in adhesion, in the actual applications, can prolong the service life of relevant equipment.

3. Materials and Methods

3.1. Sample Preparation

Copper sheets (Dongguan Tongrun Copper and Aluminum Materials Co., LTD., Dongguan, China) at a thickness of 1.0 mm and a diameter of 20.0 mm were used in the experiment. Before the laser texturing, the samples were polished using 1500# and 2000# SiC sandpapers and then cleaned in anhydrous ethanol (Analytical pure, Xilong Scientific Co., LTD., Shantou, China) and deionized water ultrasonically for 10 min. The process of sample preparation is shown in Figure 1. The substrates were ablated in ambient air by a UV laser (JPT-SEAL-355-5, JPT Laser Co., LTD, Shenzhen, China) at a repetition rate of 60 kHz and a pulse duration of 5 ns. The wavelength of the used laser was 355 nm and the spot size was 15 μm . The focused laser beam scanned the surfaces in the desired patterns under the control of a galvanometer scanning system. The scanning pattern vertically intersected lines with different intervals (30, 50 and 60 μm) to construct micro-column arrays. The size of processed area was 10 \times 10 mm^2 . The parameters of laser texturing included a laser fluence of 8.3 J/cm^2 , a scanning speed of 500 mm/s , and a scanning pass of 20. Then, a group of samples was heated for 2, 4, and 6 h to grow CuO nanowires. The textured samples were placed on a heating plate and thermally oxidized at 550 $^\circ\text{C}$ and cooled at 4 $^\circ\text{C}/\text{min}$ down to room temperature. This group sample was named LT-TO (laser texturing—thermal oxidation), for example, 30LT-2TO represented the sample treated by the laser scanning interval of 30 μm and thermal oxidation time for 2 h. The other group of samples was processed by coupling the laser post-treatment between the laser texturing and thermal oxidation as shown in Figure 1. In the laser post-treatment, the scanning pattern vertically intersected lines with an interval of 20 μm to cover the whole surface. The parameters of the laser post-treatment included a laser fluence of 6.2 J/cm^2 and a scanning pass of 2. This group sample was named LT-LPT-TO (laser texturing—laser post-treatment—thermal oxidation), for example, 50LT-LPT-4TG represented the sample treated by the laser scanning interval of 50 μm , laser post-treatment, and thermal oxidation for 4 h. Finally, all samples were treated with isopropyl alcohol (IPA) to obtain low surface energy. The surface chemical property was attributed to surface wettability. According to our previous work [44,45], the transition time from hydrophilicity to hydrophobicity was about 2 weeks as a result of the absorption and accumulation of organic substances on the textured surface when exposed to ambient air. It could be shortened by immersion into IPA for a period of 3 h.

3.2. Surface Characterization

The surface morphology was characterized by a scanning electron microscope (SEM) (SUPRA 55, ZEISS, Oberkochen, Germany) equipped with energy dispersive spectroscopy (EDS) (X-MAX 80, OXFORD Instruments, Shanghai, China). The depths of texture were measured by a super-depth-of-field microscope (VHX-5000, Keyence, Osaka, Japan). The density of CuO nanowires was evaluated via ImageJ software. The contact angle (CA) and sliding angle (SA) were measured by a video-based optical instrument (JC2000D, Shanghai Kuncheng Scientific Instrument Co., LTD, Shanghai, China) with 5 μL deionized water droplets at room temperature. The CA and SA of each sample were measured 5 times and the average value was adopted.

3.3. Anti-Icing Performance Evaluation

The anti-icing performances were characterized by recording a single droplet freezing process. The experiment was conducted at the ambient temperature of 24 $^\circ\text{C}$. The samples were placed on a homemade low-temperature platform by a thermoelectric cooler to control the surface temperature at -10 $^\circ\text{C}$. To ensure constant temperature and humidity, the sample test platform was placed in a closed transparent acrylic box, which was isolated from the outside atmosphere. The volume of the deionized droplet was 7 μL . The whole freezing process of the droplet was recorded by a mobile phone (iPhone 12 Pro Max, Apple, CA, USA).

3.4. Durability Evaluation

The icing–melting cycles and tape tests were used to assess the durability of the samples. The water droplet was frozen and melted, then removed by a compressed air spray gun as one cycle of test. The water was dropped on the center of processed area to minimize errors. A total of 10 cycles were repeated to observe the changes in wettability and delayed freezing time. The standard adhesive tape (3M Scotch Tape, 3M China Co., LTD, Shanghai, China) was attached to the sample surfaces by applying certain pressure stress of 2 N/cm². Then, the tape was removed at a slow speed of 20 cm/s. The sample wettability was characterized after each cycle; 10 cycles were repeated as a complete test.

4. Conclusions

In this study, much richer CuO nanowires have been fabricated by the addition of the laser post-treatment between laser texturing and thermal oxidation. Based on the characterizations of surface morphologies, wettability, anti-icing performance, and durability, it can be concluded that the Cu₂O and CuO layers induced by the laser post-treatment promote the distribution and the growth of CuO nanowires on the surface. The density of CuO nanowires increases from 44.3% to 61.4% with a superhydrophobic property at a contact angle of 164° and sliding angle of 2°. The sample shows valuable anti-icing performance by delaying freezing time of a single droplet from 17 s to 1519 s at the temperature of −10 °C, which is more than 80 times longer compared to pure Cu. By icing–melting cycles and the tape test, the nanowires have been proven to bind firmly onto the substrate, improving the durability of surface functions. The presented method improves the thermal growth of CuO nanowires on the surface of the copper substrate and further obtains excellent superhydrophobic and anti-icing properties, which is of great significance to extend the applications of CuO nanowires, especially in a low-temperature environment.

Supplementary Materials: The following supporting information can be downloaded at: <https://www.mdpi.com/article/10.3390/inorganics10120236/s1>, Figure S1: SEM images of surface morphologies at different magnifications and laser texturing intervals (thermal oxidation time is 4 h) (a) without and (b) with the laser post-treatment; Figure S2: SEM images of surface morphologies at different magnifications and thermal oxidation time (laser texturing intervals is 50 μm); Figure S3: SEM images of surface morphologies at an oblique view with the laser post-treatment; Figure S4: SEM images of surface morphologies at different laser texturing intervals without the laser post-treatment; Figure S5: SEM images of surface morphologies at different laser texturing intervals with the laser post-treatment; Figure S6: Ultra-depth-of-field microscope image of samples with and without laser post-treatment; Figure S7: Statistical SEM images of density of nanowires on different samples with and without laser post-treatment.

Author Contributions: Conceptualization, Z.C. and M.H.; methodology, Z.C., G.Y., W.H. and M.H.; software, Z.C. and G.Y.; validation, R.Z. and M.H.; formal analysis, R.Z.; investigation, Z.C. and G.Y.; resources, R.Z. and M.H.; data curation, Z.C., G.Y. and W.H.; writing—original draft preparation, Z.C. and G.Y.; writing—review and editing, R.Z. and M.H.; visualization, Z.C. and W.H.; supervision, R.Z. and M.H.; project administration, R.Z. and M.H.; funding acquisition, R.Z. and M.H. All authors have read and agreed to the published version of the manuscript.

Funding: This research was funded by [National Natural Science Foundation of China] grant number 62175203, [Fujian Provincial Science and Technology Programme] grant number 2020H0006, and [Innovation Laboratory for Sciences and Technologies of Energy Materials of Fujian Province Applied Research Project] grant number RD2020050301.

Acknowledgments: The support by China Scholarship Council (CSC) during a visit of Zhekun Chen to National University of Singapore is acknowledged.

Conflicts of Interest: The authors declare no conflict of interest.

References

1. Abdulshaheed, A.A.; Wang, P.; Huang, G.; Li, C. High performance copper-water heat pipes with nanoengineered evaporator sections. *Int. J. Heat Mass Transf.* **2019**, *133*, 474–486. [[CrossRef](#)]
2. Yoon, B.Y.; Jung, G.; Lim, C.S. A Study on the Corrosion of Cu-Ni Alloy in Chlorinated Seawater for Marine Applications. *Corros. Sci. Technol.* **2018**, *17*, 176–182.
3. Long, J.; Wu, Y.; Gong, D.; Fan, P.; Jiang, D.; Zhang, H.; Zhong, M. Femtosecond Laser Fabricated Superhydrophobic Copper Surfaces and Their Anti-Icing Properties. *Chin. J. Lasers* **2015**, *42*, 706002. [[CrossRef](#)]
4. Jiang, W.; He, J.; Xiao, F.; Yuan, S.; Lu, H.; Liang, B. Preparation and Antiscaling Application of Superhydrophobic Anodized CuO Nanowire Surfaces. *Ind. Eng. Chem. Res.* **2015**, *54*, 6874–6883. [[CrossRef](#)]
5. Shu, Y.; Zhang, Y.; Zhang, J. First-principles analysis of properties of Cu surfaces. *Acta Phys. Sin.* **2012**, *61*, 016108. [[CrossRef](#)]
6. Liang, C.; Lin, K.; Cheng, P. Effect of Au/Pd bilayer metallization on solder/Cu interfacial reaction and growth kinetics of Cu Sn intermetallic compounds during solid-state aging. *Surf. Coat. Technol.* **2017**, *319*, 55–60. [[CrossRef](#)]
7. Vogel, G. Creeping corrosion of copper on printed circuit board assemblies. *Microelectron. Reliab.* **2016**, *64*, 650–655. [[CrossRef](#)]
8. Oh, G.H.; Joo, S.J.; Jeong, J.W.; Kim, H.S. Effect of plasma treatment on adhesion strength and moisture absorption characteristics between epoxy molding compound/silicon chip (EMC/chip) interface. *Microelectron. Reliab.* **2019**, *92*, 63–72. [[CrossRef](#)]
9. Nekouei, R.K.; Pahlevani, F.; Rajarao, R.; Golmohammadzadeh, R.; Sahajwalla, V. Two-step pre-processing enrichment of waste printed circuit boards: Mechanical milling and physical separation. *J. Clean. Prod.* **2018**, *184*, 1113–1124. [[CrossRef](#)]
10. Zou, S.; Li, X.; Dong, C.; Ding, K.; Xiao, K. Electrochemical migration, whisker formation, and corrosion behavior of printed circuit board under wet H₂S environment. *Electrochim. Acta* **2013**, *114*, 363–371. [[CrossRef](#)]
11. Huang, Z.; Zhou, Y.; He, W. A combination of self-assembled monolayer and hydrophobic conformal coating for anti-corrosion of Cu/NiP/Au 3D circuitry in artificial sweat solution. *Surf. Coat. Technol.* **2017**, *320*, 126–131. [[CrossRef](#)]
12. Ghosh, S. Three-dimensional microplate formation with evaporating nanoparticle suspensions on superhydrophobic surfaces. *Colloids Surf. A Physicochem. Eng. Asp.* **2017**, *529*, 901–906. [[CrossRef](#)]
13. Han, L.; Zhao, X.; Shen, Y. Study of the effect of thermal conductivity on the anti-icing performance of coated fabrics. *Text. Res. J.* **2020**, *90*, 2035–2045. [[CrossRef](#)]
14. Liu, C.; Liu, Q.; Jin, R.; Lin, Z.; Qiu, H.; Xu, Y. Mechanism analysis and durability evaluation of anti-icing property of superhydrophobic surface. *Int. J. Heat Mass Transf.* **2020**, *156*, 119768. [[CrossRef](#)]
15. Zhu, K.; Li, X.; Su, J.; Li, H.; Zhao, Y.; Yuan, X. Improvement of anti-icing properties of low surface energy coatings by introducing phase-change microcapsules. *Polym. Eng. Sci.* **2018**, *58*, 973–979. [[CrossRef](#)]
16. Jiang, X.; Fan, C.; Xie, Y. New method of preventing ice disaster in power grid using expanded conductors in heavy icing area. *IET Gener. Transm. Distrib.* **2018**, *13*, 536–543. [[CrossRef](#)]
17. Zheng, M.; Wu, S.; Wang, C.; Li, Y.; Ma, Z.; Peng, L. A Study on Evaluation and Application of Snowmelt Performance of Anti-Icing Asphalt Pavement. *Appl. Sci.* **2017**, *7*, 583. [[CrossRef](#)]
18. Sarajcev, I.; Majstrovic, M.; Medic, I. Calculation of losses in electric power cables as the base for cable temperature analysis. *Adv. Comput. Methods Heat Transf. VI* **2000**, *3*, 529–537.
19. Mishchenko, L.; Hatton, B.; Bahadur, V.; Taylor, J.A.; Krupenkin, T.; Aizenberg, J. Design of Ice-free Nanostructured Surfaces Based on Repulsion of Impacting Water Droplets. *ACS Nano* **2010**, *4*, 7699–7707. [[CrossRef](#)]
20. Guo, P.; Zheng, Y.; Wen, M.; Song, C.; Lin, Y.; Jiang, L. Icephobic/anti-icing properties of micro/nanostructured surfaces. *Adv. Mater.* **2012**, *24*, 2642–2648. [[CrossRef](#)]
21. Li, J.; Zhou, Y.; Wang, W.; Xu, C.; Ren, L. Superhydrophobic Copper Surface Textured by Laser for Delayed Icing Phenomenon. *Langmuir* **2020**, *36*, 1075–1082. [[CrossRef](#)]
22. Chen, Z.; Zhou, R.; Yan, H.; Lin, Y.; Huang, W.; Yuan, G.; Cui, J. Bioinspired robust top-perforated micro-conical array of TC4 surface fabricated by pulsed laser ablation for enhanced anti-icing property. *J. Mater. Sci.* **2022**, *57*, 8890–8903. [[CrossRef](#)]
23. He, Z.; Zhang, Z.; He, J. CuO/Cu based superhydrophobic and self-cleaning surfaces. *Scr. Mater.* **2016**, *118*, 60–64. [[CrossRef](#)]
24. Zhan, Y.; Ruan, M.; Li, W.; Li, H.; Hu, L.; Ma, F.; Yu, Z.; Feng, W. Fabrication of anisotropic PTFE superhydrophobic surfaces using laser microprocessing and their self-cleaning and anti-icing behavior. *Colloids Surf. A Physicochem. Eng. Asp.* **2017**, *535*, 8–15. [[CrossRef](#)]
25. Liu, G.; Yuan, Y.; Liao, R.; Wang, L.; Gao, X. Fabrication of a Porous Slippery Icephobic Surface and Effect of Lubricant Viscosity on Anti-Icing Properties and Durability. *Coatings* **2020**, *10*, 896. [[CrossRef](#)]
26. Dou, W.; Wu, J.; Gu, T.; Wang, P.; Zhang, D. Preparation of super-hydrophobic micro-needle CuO surface as a barrier against marine atmospheric corrosion. *Corros. Sci.* **2018**, *131*, 156–163. [[CrossRef](#)]
27. Mirzanamadi, R.; Hagentoft, C.E.; Johansson, P. Coupling a Hydronic Heating Pavement to a Horizontal Ground Heat Exchanger for harvesting solar energy and heating road surfaces. *Renew. Energy* **2020**, *147*, 447–463. [[CrossRef](#)]
28. Kirner, S.V.; Hermens, U.; Mimidis, A.; Skoulas, E.; Florian, C.; Hischen, F.; Plamadela, C.; Baumgartner, W.; Winands, K.; Mescheder, H.; et al. Mimicking bug-like surface structures and their fluid transport produced by ultrashort laser pulse irradiation of steel. *Appl. Phys. A* **2017**, *123*, 754. [[CrossRef](#)]
29. Hu, L.; Zhang, L.; Wang, D.; Lin, X.; Chen, Y. Fabrication of biomimetic superhydrophobic surface based on nanosecond laser-treated titanium alloy surface and organic polysilazane composite coating. *Colloids Surf. A Physicochem. Eng. Asp.* **2018**, *555*, 515–524. [[CrossRef](#)]

30. Xu, K.; Yan, H.; Tan, C.F.; Lu, Y.; Li, Y.; Ho, G.W.; Ji, R.; Hong, M. Hedgehog Inspired CuO Nanowires/Cu₂O Composites for Broadband Visible-Light-Driven Recyclable Surface Enhanced Raman Scattering. *Adv. Opt. Mater.* **2018**, *6*, 1701167. [[CrossRef](#)]
31. Khew, S.; Tan, C.; Yan, H.; Lin, S.; Thian, E.; Zhou, R.; Hong, M. Nanosecond laser ablation for enhanced adhesion of CuO nanowires on copper substrate and its application for oil-water separation. *Appl. Surf. Sci.* **2019**, *465*, 995–1002. [[CrossRef](#)]
32. Yan, X.; Huang, Z.; Sett, S.; Oh, J.; Cha, H.; Li, L.; Feng, L.; Wu, Y.; Zhao, C.; Orejon, D.; et al. Atmosphere-Mediated Superhydrophobicity of Rationally Designed Micro/Nanostructured Surfaces. *ACS Nano* **2019**, *13*, 4160–4173. [[CrossRef](#)]
33. Wenzel, R. Resistance of solid surfaces to wetting by water. *Trans. Faraday Soc.* **1936**, *28*, 988–994. [[CrossRef](#)]
34. Cassie, A.; Baxter, S. Wettability of Porous Surfaces. *Trans. Faraday Soc.* **1944**, *40*, 546–551. [[CrossRef](#)]
35. Zhao, Y.; Hou, Y.S.X.; Hong, M. Directional sliding of water: Biomimetic snake scale surfaces. *Opto-Electron. Adv.* **2021**, *4*, 210008. [[CrossRef](#)]
36. Zhao, J.; Wang, D.; Chen, Y.; Jin, Q.; Wang, G. Enhanced Field Emission from UV-Illuminated CuO Nanowires Fabricated by Thermal Oxidation of Cu Film. *Nano* **2016**, *11*, 1650056. [[CrossRef](#)]
37. Zhang, Q.; Wang, J.; Xu, D.; Wang, Z.; Li, X.; Zhang, K. Facile large-scale synthesis of vertically aligned CuO nanowires on nickel foam: Growth mechanism and remarkable electrochemical performance. *J. Mater. Chem. A* **2014**, *2*, 3865–3874. [[CrossRef](#)]
38. Zhang, Q.; Xu, D.; Hung, T.; Zhang, K. Facile synthesis, growth mechanism and reversible superhydrophobic and superhydrophilic properties of non-flaking CuO nanowires grown from porous copper substrates. *Nanotechnology* **2013**, *24*, 065602. [[CrossRef](#)]
39. Cao, F.; Jia, S.; Zheng, H.; Zhao, L.; Liu, H.; Li, L.; Zhao, L.; Hu, Y.; Gu, H.; Wang, J. Thermal-induced formation of domain structures in CuO nanomaterials. *Phys. Rev. Mater.* **2017**, *1*, 053401. [[CrossRef](#)]
40. Jiang, X.; Herricks, T.; Xia, Y. CuO Nanowires Can Be Synthesized by Heating Copper Substrates in Air. *Nano Lett.* **2002**, *2*, 1333–1338. [[CrossRef](#)]
41. Shi, Y.; Yang, W.; Feng, X.; Feng, L.; Yue, G.; Wang, Y. Bio-inspired fabrication of copper oxide nanowire films with switchable wettability via a facile thermal oxidation method. *RSC Adv.* **2015**, *5*, 26107–26113. [[CrossRef](#)]
42. Zhang, K.; Rossi, C.; Tenailleau, C.; Alphonse, P.; Chane-Ching, J.Y. Synthesis of large-area and aligned copper oxide nanowires from copper thin film on silicon substrate. *Nanotechnology* **2007**, *18*, 275607. [[CrossRef](#)]
43. Fraggelakis, F.; Tsibidis, G.D.; Stratakis, E. Ultrashort pulsed laser induced complex surface structures generated by tailoring the melt hydrodynamics. *Opto-Electron. Adv.* **2022**, *5*, 210052. [[CrossRef](#)]
44. Tang, M.; Shim, V.; Pan, Z.Y.; Choo, Y.S.; Hong, M.H. Laser ablation of metal substrates for super-hydrophobic effect. *J. Laser Micro Nanoeng.* **2011**, *6*, 6. [[CrossRef](#)]
45. Yan, H.; Rashid, M.R.; Khew, S.Y.; Li, F.; Hong, M. Wettability transition of laser textured brass surfaces inside different mediums. *Appl. Surf. Sci.* **2018**, *427*, 369–375. [[CrossRef](#)]